applied sciences

MDPI

Article

Pharmacoinformatics, Molecular Dynamics Simulation, and Quantum Mechanics Calculation Based Phytochemical Screening of *Croton bonplandianum* Against Breast Cancer by Targeting Estrogen Receptor-α (ERα)

Shuvo Saha [1,†], Partha Biswas [2,†], Mohaimenul Islam Tareq [2], Musfiqur Rahman Sakib [3], Suraia Akter Rakhi [4], Md. Nazmul Hasan Zilani [5], Abdel Halim Harrath [6], Md. Ataur Rahman [7,*] and Md. Nazmul Hasan [2,*]

1 Department of Genetic Engineering and Biotechnology, Jashore University of Science and Technology, Jashore 7408, Bangladesh; shuvo.ge@gmail.com
2 Laboratory of Pharmaceutical Biotechnology and Bioinformatics, Jashore University of Science and Technology, Jashore 7408, Bangladesh; partha_160626@just.edu.bd (P.B.); 180611.gebt@student.just.edu.bd (M.I.T.)
3 Department of Pharmacy, Bangabandhu Sheikh Mujibur Rahman Science and Technology University, Gopalganj 8100, Bangladesh; 16phr027@bsmrstu.edu.bd
4 Department of Applied Chemistry and Chemical Engineering, Bangabandhu Sheikh Mujibur Rahman Science and Technology University, Gopalganj 8100, Bangladesh; suraia.16ace025@bsmrstu.edu.bd
5 Department of Pharmacy, Jashore University of Science and Technology, Jashore 7408, Bangladesh; zilani.phar@just.edu.bd
6 Department of Zoology, College of Science, King Saud University, Riyadh 11451, Saudi Arabia; hharrath@ksu.edu.sa
7 Department of Oncology, Karmanos Cancer Institute, School of Medicine, Wayne State University, Detroit, MI 48201, USA
* Correspondence: ataur1981rahman@hotmail.com (M.A.R.); mn.hasan@just.edu.bd (M.N.H.)
† These authors contributed equally to this work.

Abstract: Breast cancer progression is strongly influenced by estrogen receptor-α (ERα), a ligand-activated transcription factor that regulates hormone binding, DNA interaction, and transcriptional activation. ERα plays a key role in promoting cell proliferation in breast tissue, and its overexpression is associated with the advancement of breast cancer through estrogen-mediated signaling pathways. Targeting ERα is, therefore, a promising therapeutic strategy for breast cancer. However, there are currently no phytochemical-based drug candidates approved for effectively inhibiting breast cancer progression driven by elevated ERα expression. This study aims to identify phytochemical inhibitors from *Croton bonplandianum* against ERα using pharmacoinformatics approaches. Eighty-three bioactive compounds from *C. bonplandianum* were retrieved from the IMPPAT (Indian Medicinal Plants, Phytochemistry, and Therapeutics) database and screened through molecular docking for their binding affinity to ERα. The top candidates were further evaluated through molecular dynamics simulations, ADME analysis, toxicity assessment, and quantum mechanics-based DFT calculations. The thermodynamic properties and HOMO-LUMO energy gap values indicated that the selected compounds were both stable and active. Among them, 2,3-oxidosqualene (CID-5366020) and 5,8,11-eicosatriynoic acid, trimethylsilyl ester (CID-91696396) demonstrated the most potent inhibitory activity against ERα. These findings suggest that these compounds have significant potential as therapeutic agents for breast cancer treatment by targeting ERα.

Keywords: breast cancer; estrogen receptor-α; *Croton bonplandianum*; molecular docking; ADMET; DFT; molecular dynamics simulation

check for updates

Citation: Saha, S.; Biswas, P.; Tareq, M.I.; Rahman Sakib, M.; Akter Rakhi, S.; Zilani, M.N.H.; Harrath, A.H.; Rahman, M.A.; Hasan, M.N. Pharmacoinformatics, Molecular Dynamics Simulation, and Quantum Mechanics Calculation Based Phytochemical Screening of *Croton bonplandianum* Against Breast Cancer by Targeting Estrogen Receptor-α (ERα). *Appl. Sci.* **2024**, *14*, 9878. https://doi.org/10.3390/app14219878

Academic Editor: Luca Cattelani

Received: 2 September 2024
Revised: 19 October 2024
Accepted: 22 October 2024
Published: 29 October 2024

Copyright: © 2024 by the authors. Licensee MDPI, Basel, Switzerland. This article is an open access article distributed under the terms and conditions of the Creative Commons Attribution (CC BY) license (https://creativecommons.org/licenses/by/4.0/).

1. Introduction

Breast cancer (BC) is a distinct form of malignant tumor originating from the cells within the breast tissue that results in the death of women all over the world, and it is one

of the most significant health concerns in the modern era [1,2]. According to the published epidemiological data, the death rates because of this cancer have risen dramatically in the last two decades throughout the world [3]. Breast cancer claimed the lives of nearly 685,000 people globally in 2020, of which 0.5–1% occurred in men. Furthermore, data from the five years prior to 2020 indicated that, as of the end of that year, there were 7.8 million women diagnosed with BC who were still alive. In 2020, more than 2.3 million women had this sort of cancer diagnosis. These statistics demonstrate the disease's mortality rate, which makes it the most prevalent cancer type worldwide [4]. By the year 2050, it is anticipated that there will be 3.2 million new cases of breast cancer diagnosed in women globally each year [5–7]. This demonstrates the deadly global impact of this cancer on individuals and underscores the critical need for diagnosis and treatment. As of present, there are no specific pharmaceutical interventions available for the disease. The progression in comprehending the disease's pathophysiology has expanded treatment modalities, including surgery, chemotherapy, and adjuvant radiotherapy, aimed at curing the ailment. Nonetheless, a major challenge in treatment remains the development of chemotherapeutic resistance. For example, Anthracyclines, recognized as a cornerstone in treatment, demonstrate significant efficacy in enhancing survival rates. Nevertheless, their utilization is hindered by enduring toxicities such as cardiotoxicity and hematologic malignancies, particularly in elderly patients with breast cancer [8]. Moreover, resistance to Anthracyclines frequently emerges, leaving limited therapeutic alternatives once resistance develops [9]. Patients with estrogen receptor α (ERα) positive breast cancer also reflect this type of resistance. One mechanism associated with the resistance to chemotherapeutic drugs is the epithelial–mesenchymal transition (EMT), characterized by the loss of epithelial cell polarity and decreased cell adhesion [10]. The global prevalence of breast cancer has surged significantly in recent years, underscoring the critical need for identifying novel therapeutic candidates.

Estrogen contributes to normal development and growth, as well as diseases in the skeleton, breasts, and uterus. There are two subtypes of estrogen receptors, which are denoted by the ERα (estrogen receptor-α) and Erβ (estrogen receptor-β) [11]. Endometrial cells, mammary epithelial cells, which are the growth-initiating cells in the vast majority of breast cancers, ovarian stromal cells, and the hypothalamus all contain ER, which has been found to play a substantial part in the process of cell proliferation in all of these tissues [12,13]. Because ER is the most prevalent risk factor for developing breast cancer, it plays an important and significant part in the evolution of the disease [14–16]. Today, patients with estrogen-dependent breast cancer (EDBC) or hormone-dependent breast cancer (HDBC) are treated based on medical, histological, and hormonal receptor (HER2, ER, PR) criteria [17]. In breast cancer, individuals whose malignancies were ER-positive had a better prognosis than patients whose tumors were ER-negative [18]. Furthermore, after evaluating the literature, we observed that 70 to 75% of breast tumors express positive estrogen receptors alpha (ERα), with the causative receptors being ER-positive (ER+) [19–22].

Phytochemicals have been widely used since ancient times and display a broad spectrum of protective effects against various forms of diseases [23]. These naturally occurring chemical compounds represent a promising class of therapeutics for the treatment of various diseases, including cancer [24]. One such plant, *Croton bonplandianum,* is widely recognized for its versatile therapeutic efficacy in different diseases as an alternative but effective medicinal system. The phytoconstituents from this medicinal plant show effective antioxidant, antimicrobial, anti-fungal, genotoxic, anti-tumor, cytotoxic, and pro-apoptotic activity [25–29]. Despite its efficacy, there is currently no reported evidence of the effectiveness of compounds derived from this plant as inhibitors against the ERα protein for the treatment of breast cancer.

The discovery of natural sources as effective anticancer drugs is hampered by limitations in the characterization of phytocompounds and the development of successful assays to assess therapeutic efficiency by traditionally assessing potential targets. The practice of developing drugs in silico has gained popularity outside of the traditional drug

discovery procedure [30]. The extraction and characterization of natural compounds for the development of anticancer drugs often include some inevitable obstacles and require a significant amount of time [31]. With the help of bioinformatic online servers and tools, the computational structure-based inhibitor screening approach has revolutionized the drug discovery process by accelerating the process through the use of molecular docking, molecular dynamic simulation, and ADMET (absorption, distribution, metabolism, excretion, and toxicity) analyses [32–34]. As a result of its specificity and efficiency in locating and refining new lead compounds, this approach has enabled us to advance our existing knowledge of the development of novel therapies [35]. Extraction and characterization of each natural compound from the source for the development of anticancer drugs are typically difficult and time-consuming due to insurmountable obstacles [36]. Contrarily, computer-aided drug design (CADD) overcomes such obstacles and accelerates the process of quickly screening, characterizing, and evaluating potential therapeutic candidates [37]. Treatments for various diseases can be discovered through CADD investigation, which employs molecular docking and molecular dynamics (MD) simulation techniques [38]. Molecular docking analysis facilitates the initial screening of therapeutic candidates to the intended target based on their binding affinity for draggable ligands [39]. Similarly, in a synthetically generated computer environment that approximates the human body, molecular dynamics simulations (MDS) allow us to determine the stability of protein–ligand binding interactions [40]. To select through the possible drug candidates from *Croton bonplandianum* as a therapeutic option against breast cancer, this research used computational drug design methodologies.

2. Materials and Methods

2.1. Compounds Retrieval and Preparation

A total of 83 phytochemicals were extracted from *Croton bonplandianum* due to their anticancer properties, sourced from the IMPPAT (Indian Medicinal Plants, Phytochemistry, and Therapeutics) database (Table S1). IMPPAT is a manually curated database that provides cheminformatic tools to facilitate the discovery of natural bioactive therapeutics, with over 9500 phytochemicals and more than 1742 Indian medicinal plants [41]. A spatial data file (SDF) file of all ligands along with the control drug, retrieved from the PubChem database (https://pubchem.ncbi.nlm.nih.gov/, accessed on 2 March 2024), were prepared using the LigPrep tools of the Schrödinger program (https://www.Schr%C3%B6dinger.com/products/maestro, accessed on 4 March 2024). With an RMSD of 1.0 and a maximum of 32 conformers for each structure, the minimizing technique was applied using the OPLS3e force field and the Epik ionizer at a pH range of 7.0 to (±2.0).

2.2. Pharmacokinetics Properties of Compounds

AdMET is used to predict pharmacokinetic factors of druggable phytocompounds, such as absorption, distribution, metabolism, excretion, and toxicity. The Swiss ADME (http://www.swissadme.ch/, accessed on 14 March 2024) was used to assess 83 ligands with the evaluation of logP values as well as other parameters [42]. Afterward, the toxicity of various potential antagonists was investigated using pKCSM (http://biosig.unimelb.edu.au/pkcsm/prediction, accessed on 15 March 2024).

2.3. Thermodynamic Properties of the Compounds

Investigations were conducted on the fundamental thermodynamic properties of the subject, as well as its changes, using Gaussian 6.0.16 and the B3LYP/6-31G(d, p) level of density functional theory (DFT) [43]. These analyses involved energy estimations, structural optimizations, and the determination of the molecular geometry for the newly generated structures.

2.4. FMO of the Compounds

The FMO concept, usually known as Frontier molecular orbital theory, represents one type of molecular orbital theory that examines how its two parameters, HOMO and LUMO, intersect. Afterward, the reactivity index for substances that have been suggested as potential prospective medicinal possibilities is determined. A variety of factors influence sensitivity, including the bandgap frequency between HOMO and LUMO (E_g); chemical hardness (η), which is determined by splitting overall distance through two; chemical softness (S), which represents its reciprocal to its hardness; and molecule's electrostatic potential. All calculations were performed using Schrödinger Release 2021-2: Materials Science Suite, Schrödinger, NY, USA, 2020-3. Greater polar substances, as well as antagonists, include those with larger dipole moments [44–46]. The dipole potential is created by combining asymmetrically opposing energies within the molecules, strengthening individual substances' ability to form ionic bonding [47]. To create various sensitivity indices, several subsequent formulae were utilized:

$$E_g = E_{LUMO} - E_{HOMO}$$

$$IP = -E_{HOMO}$$

$$EA = -E_{LUMO}$$

$$\eta = \frac{(E_{LUMO} - E_{HOMO})}{2}$$

$$\mu = \frac{(E_{LUMO} + E_{HOMO})}{2}$$

$$S = \frac{1}{\eta}$$

2.5. Molecular Docking and Post-Docking Visualization

The 3D experimental tertiary structure of the target protein was retrieved from the Research Collaboratory for Structural Bioinformatics Protein Data Bank (RCSB PDB) and used as the receptor complex in molecular docking analysis. The Protein Preparation Wizard 12.5 was employed to preprocess the protein, with Prime selected for creating disulfide bonds, establishing zero-order bonds with metals, and optimizing disulfide bonds. Additionally, the Epic application was utilized to generate protonation states at varying pH levels, ranging from 7.0 to 2.0 [48]. The receptor grid was constructed, focusing on the active site indicated by the protein's native ligand. The optimal lead compounds underwent site-specific XP molecular docking analysis using Maestro (Schrödinger Release 2021-2: Maestro, Schrödinger, LLC, New York, NY, USA, 2020-3). The PDB format of each protein–ligand complex was obtained from post-viewing files of molecular docking trajectories. These complexes were subsequently utilized for post-docking visualization analysis aimed at exploring non-bond interactions and assessing bioactivity and hydrophobicity. Following site-specific XP molecular docking analysis, the combined PDB structure comprising the targeted protein and chosen ligand compounds was extracted for post-docking examination. Non-covalent interactions within receptor–ligand structural complexes were scrutinized using the Maestro post-docking visualization tool featuring a Java interface. Additionally, Discovery Studio Visualizer 64-bit was employed to confirm the integrity of structural bonds, as well as the polar and non-polar interactions within the complexes, along with other relevant characteristics [49].

2.6. Molecular Dynamics Simulation (MDS)

To assess the potential ligand molecules' uniformity for interacting with the targeted 3ERT protein model, Schrödinger's "Desmond v3.6 Programme" (https://www.Schr%C3%B6dinger.com/, accessed on 15 March 2024) (Paid version) was utilized within a Linux framework to perform molecular dynamic simulations evaluating various protein–ligand

complex structures [50]. The two prospective ligand molecules that were selected for testing were CID-250006068, CID-5366020, CID-91696396, CID-7311, and CID-23725625 (control). Within this framework, the orthorhombic periodic bounding box shape separated across a space of 10 Å is contained in a specified volume established by the prescribed TIP3P aqueous technique. To neutralize electric power in its structure, recommended ions were selected and randomly distributed throughout its chemical solvent environment, such as Na^+ and Cl^- from 0+ and 0.15 M salt. The system's framework was later decreased and made more pleasant using the procedure carried out by applying force field constants OPLS3e provided within the Desmond package once the necessary protein structures containing agonist combinations were built. Every Isothermal–Isobaric ensemble (NPT) assembly, which used an efficacy of 1.2 kcal/mol and overall Nose–Hoover temperature combinations and its isotropic technique, was followed by 50 PS grabbing pauses and contained approximately 300 K and one atmospheric pressure (1.01325 bar). We assessed the overall accuracy of this MD simulation using the Simulations Interaction Diagram (SID) from the Desmond modules of the Schrödinger suite. The stability of the protein–ligand complex was evaluated by analyzing data related to protein–ligand interactions (P-L), intramolecular hydrogen bonds, solvent-accessible surface area (SASA), the radius of gyration (Rg), molecular surface area (MolSA), and polar surface area (PSA).

2.6.1. Simulation Trajectory Analysis

The following MD simulation images were generated using version 9.5 of Schrödinger's Maestro application. The Simulations Interaction Diagram (SID) in the Desmond module of the Schrödinger package was utilized to facilitate a potential simulation scenario and evaluate the accuracy of the MD simulation. To analyze the stability of the protein–ligand complex structure based on trajectory efficiency, we employed the following metrics: root mean square deviation (RMSD), protein–ligand contacts (P-L), intramolecular hydrogen bonds, solvent accessible surface area (SASA), a radius of gyration (Rg), molecular surface area (MolSA), and polar surface area (PSA).

2.6.2. RMSD

The RMSD serves the average distances produced by removing one molecule from a system throughout a predetermined amount of duration in comparison to a reference value. The RMSD of protein conjugated ligand atoms was calculated over every time frame, which is coordinated and assessed against the benchmark time, and was added after the RMSD of protein structural atoms, including C, foundation, sidechain, as well as bulkier elements. When running an MD simulation over a certain time x, the RMSD can be determined using the following equation (Equation (1)).

$$RMSDx = \sqrt{\frac{1}{N}} \sum_{i=1}^{N} \left(r\prime i\ (t_x) - r_i\ \left(t_{ref}\right)\right)^2 \quad (1)$$

After completing the setup of the reference system, the position of the selected atom is indicated by the symbol r', and the entire system has been overlaid on system x. N is the total number of atoms considered, along with three additional terms and t_{ref}, which stands for the time interval.

2.6.3. RMSF

Regarding the protein complex, the RMSF was mostly utilized to detect and track regional alterations in translational structure. Using the continuity formula, one may obtain the RMSF frequency in an MD simulation of amino acid with residue count i (Equation (2)).

$$RMSF_i = \sqrt{\frac{1}{T}} \sum_{t=1}^{T} < \left(r\prime i\ (t) - r_i\ \left(t_{ref}\right)\right)^2 > \quad (2)$$

For this RMSF calculation, T represents the time along the trajectory. "t_{ref}" denotes the reference time, "r_i" represents the location of residue i, and "r'" signifies the position of residue i atoms assuming superposition at the reference time. The angle brackets denote that the square distance is averaged over several atoms in the residue.

3. Results

3.1. Construction of a Ligands Library

The phytochemical components of *Croton bonplandianum* were identified and retrieved using the Indian Medicinal Plants, Phytochemistry, and Therapeutics (IMPPAT) ingredient database, as well as the PubChem databases. A total of 83 different compounds were discovered via the use of the information databases mentioned in Table S1 earlier. The smile IDs of the phytochemicals were used to do an investigation on PubChem Server, and the results were stored in an SDF file format.

3.2. Pharmacokinetics Analysis

There is currently a variety of paid and free software for analyzing the physiochemical criteria and ADMET (absorption, distribution, metabolism, elimination, and toxicity) properties. Still, we used Swiss ADME for the physiochemical criteria of drug-like compounds. In addition, the pKCSM web-based application was chosen for this project due to its flexibility and data integrity in the scientific community. However, the most effective compounds, CID-7311, CID-5366020, CID-91696396, CID-250006068, and CID-23725625 (control), are probable chemicals. Their molecular masses are 434.46, 206.32, 426.72, 372.62, and 498.89 g/mol, accordingly. Their maximum number among Lipinski principal violations (1) was imparted by both as their compound, which also had an identical bioavailability score (0.55) as well as zero AMES toxicity. Significant drugs had the least topologically polarized surface size when compared to reference medicines (control). Herein, it is also emphasized that these substances have not caused any liver damage. The LD_{50} for the substances observed in rats ranges between 1.622 and 2.623; however, its highest tolerated dosage (log mg/kg/day) in humans is between 0.200 and 0.570. Its anticipated octanol/water partitioning coefficient (Log P) ranged from 0.20 to 1.50 for investigated agents, while experimental total clearance (TC) readings ranged from 0.001 to 0.750 (log ml/min/kg). Rotatable bonds, hydrogen bond donors, hydrogen bond acceptors, and other terms are explicitly shown in Table 1.

Table 1. Pharmacokinetics analysis of the compounds.

Compounds	Mwe (g/mol)	HBA	HBD	Num Rot	T.P.S.A. (Å^2)	Log P	S.B.	LD_{50}	HpT	AT	MToD	Lp. Violation	ToC
CID-23725625 (Control)	434.46	5	1	6	86.37	2.78	0.55	2.623	Yes	No	0.204	0	0.569
CID-7311	206.32	1	1	2	20.23	3.99	0.55	2.351	No	No	0.421	0	0.759
CID-5366020	426.72	1	0	15	12.53	8.55	0.55	1.622	No	No	−0.319	1	1.396
CID-91696396	372.62	2	0	11	26.30	6.40	0.55	1.874	No	No	−0.571	1	1.702
CID-250006068	498.89	4	0	22	44.76	8.41	-	2.262	No	No	−0.097	1	1.598

Molecular weight (Mwe); number of hydrogen bond acceptors (HBA); number of hydrogen bond donors (HBD); number of rotatable bonds (Num. rot.); topological polar surface area (T.P.S.A.); predicted octanol/water partition coefficient (Log P); score of bioavailability (S.B.); oral rat acute toxicity (LD_{50}); blood–brain barrier capacity (BBB); hepatotoxicity (HpT); amount of AMES toxicity (AT); The amount of maximum tolerated dose for human (MToD); values of total clearance (ToC).

3.3. Analysis of Thermodynamic Properties of the Phyto-Compounds

To learn how modifications to the parent molecule impact therapeutic properties (electronic energy, Gibbs free energy, and enthalpy), the dipole moment, charge distribu-

tion, and thermodynamics were examined using Gaussian 6.0.16. Gaussian computations yielded a stoichiometry that revealed the original drug's chemical formula and structurally comparable derivatives. All the compounds show significant thermodynamic features. As evidenced by the outcome, the estimated dipole moment of the modified medicines was updated. Increasing the dipole moment enhances the drug–receptor complexes' polarity, hydrogen bonding, and non-bonded interactions. The binding partner's free energy is crucial for predicting their interactions. A negative value of free energy is necessary for dynamic engagement and collisions to occur, even though a positive value of free energy indicates that binding will remain relatively constant. The free energy of all the compounds was negative. To ascertain how alterations with overall parent molecules affect therapeutic qualities (electronic power, Gibbs free energy, and enthalpy), thermodynamics, charge distribution, and overall dipole moment have all been analyzed using Gaussian 6.0.16. The stoichiometry, which was generated by Gaussian computations, revealed the chemical makeup of the primary drug and its functionally comparable substitutes. In contrast to CID-23725625 (control drug), most additional metabolites exhibit noteworthy thermodynamic characteristics. These results showed that this predicted dipole moment during these changed drugs significantly revised. Overall polarity, hydrogen bonds, and the non-bond relationship among its drug–receptor assemblages are intensified while their dipole moment becomes increased. Since predicting these encounters, binding associate free energy becomes a crucial factor. Although an electric current free energy amount indicates the bindings will stay mostly steady, dynamic engagements involving impacts necessitate a decrease in the free energy magnitude. Each of the substances has negative free energy. Furthermore, these have overall thermodynamic properties, which give us the knowledge they require to comprehend the overall nature of molecules. The table indicates that to bind, both the compound and its receptor molecule have negative electronic energies. CID-7311 has the least negative −621.660 Hartree, and CID-91696396 has the highest adverse −1337.485 Hartree, which demonstrates the reason the agonist CID-91696396 has shown noteworthy binding connections alongside 3ERT. Additionally, the agonists must become increasingly more polar as the dipole moment rises. Although CID-7311 possesses the greatest dipole moment (1.335 Debye), and CID-250006068 has the most prominent dipole moment (2.014 Debye), as well as 5366020 encompassing the highest dipole moment (1.859 Debye), agonist 23725625 (control) remains the most declaring due to its ultimate dipole moment of 2.889 Debye, as well as its electronic properties along with enthalpy (Table 2).

Table 2. The values of electronic and thermodynamic features study.

Name	Stoichiometry	Electronic Energy (Hartree)	Enthalpy (Hartree)	Gibbs Free Energy (Hartree)	Dipole Moment (Debye)
CID-23725625 (Control)	$C_{24}H_{23}FN_4O_3$	−685.636	−685.635	−685.687	2.889
CID-7311	$C_{14}H_{22}O$	−621.660	−621.659	−621.719	1.335
CID-5366020	$C_{30}H_{50}O$	−1247.741	−1247.740	−1247.859	1.859
CID-91696396	$C_{23}H_{36}O_2Si$	−1337.485	−1337.484	−1337.591	1.601
CID-250006068	$C_{27}H_{54}O_4Si_2$	−1025.885	−1025.565	−1025.873	2.014

3.4. FMO Analysis of the Compounds

Frontier orbits (FO) comprise its topmost controlled molecular orbital (HOMO) as well as the lowest unoccupied molecular orbital (LUMO). Frontier orbital metabolic rates are used to calculate chemical sensitivity and how much particular medicine clings to certain interaction receptors. Contrarily, HOMO can play a significant role in building a connection between overall technical requirements and the performance of a medical device. The energy differential between the highest occupied molecular orbital (HOMO) and the lowest

unoccupied molecular orbital (LUMO) provides insight into the chemical reactivity and stability of molecules. Specifically, a larger HOMO-LUMO gap indicates higher kinetic stability and lower chemical sensitivity, as it is energetically unfavorable for an electron transition between these orbitals. This property suggests that molecules with a larger gap are less reactive. Furthermore, the use of HOMO and LUMO frequencies relates to the concept of molecular hardness and softness, where a hard molecule has a larger gap and resists deformation or reactivity, while a soft molecule has a smaller gap and is more prone to chemical interactions. This framework is commonly employed in the analysis of material properties. The following equation has been utilized to determine the drugs' hardness (η) as well as softness (S) using the Parr as well as Pearson comprehension of DFT as well as using Koopmans theorem.

$$\eta = [\varepsilon LUMO - \varepsilon HOMO]/2s = 1/\eta$$

The kinetics of this molecule govern its overall chemical persistence. The frequency variance between the HOMO and LUMO is used to determine their kinetic instability and chemical responsiveness. As the overall variation and distance between the HOMO and LUMO increase, the overall kinetic durability strengthens as the overall hardness escalates. Their gap amongst these decreases while their softness values increase, yielding decreased kinetic durability although high chemical sensitivity. The control drug 23725625 possesses a softness (S) grade of 9.803, and between every additional derivative, CID-7311 has the highest softness grade (9.900), suggesting that it possesses the chemical versatility to react during specific 3ERT (Table 3).

Table 3. HOMO-LUMO, softness and hardness studies of the compounds. Higher occupied molecular orbital (εHOMO); lower unoccupied molecular orbital (εLUMO); difference between HOMO and LUMO (Gap); hardness of the compound (H); softness of the compound (S).

Molecules (Chair)	εHOMO	εLUMO	Gap	H (Hardness, Gap/2)	S (Softness, 1/Hardness)
23725625 (Control)	−0.207	−0.002	0.205	0.102	9.803
7311	−0.208	−0.005	0.203	0.101	9.900
5366020	−0.215	−0.002	0.213	0.106	9.433
91696396	−0.239	−0.008	0.231	0.115	8.695
250006068	−0.314	−0.005	0.309	0.154	6.493

3.5. Site-Specific Molecular Docking

Our analysis discovered that the four picked phytocompounds, together with the control drug, successfully collaborate alongside the target protein ERα (estrogen receptor-α) (PDB ID: 3ERT), employing a molecular attaching approach executed via Maestro (Schrödinger Release 2021-2: Maestro, Schrödinger, LLC, New York, NY, USA, 2020-3). In contrast with the control drug olaparib (CID-23725625), the privilege of chosen biological activity substances 2,3-oxidosqualene (CID-5366020), 5,8,11-eicosatriynoic acid, trimethylsilyl ester (CID-91696396), and 1-monolinolein (CID-250006068) all demonstrated greater connecting affinities of −8.6 kcal/mol, −8.2 kcal/mol, and −8.2 kcal/mol. Nevertheless, contrasted against the chosen reference drug, this molecule 2, 4-di-tert-butylphenol (CID-7311) showed a binding ability of −7.8 kcal/mol (Table 4).

Table 4. Biochemical relationships among the intended proteins complex estrogen receptors alpha (ERα) (PDB ID: 3ERT) and the chosen phytocompounds, as measured by docking propensity scores.

Complex	Bonding Energy (kcal/mol)	H-Bond	Hydrophobic	Polar	Positive	Negative
olaparib (CID-23725625) (control drug)	−7.9		PHE 404, LEU402, LEU428, PHE425, ILE424, MET421, MET343, LEU346, LEU349, ALA350, LEU354, TRP383, LEU384, LEU387, MET388, LEU391, VAL418, GLY420, GLY521, MET522, LEU525, TYR526, MET528, CYS530, VAL533, PRO535, LEU536, LEU539	THR347 HIS524 SER527	ARG394 LYS529	ASP351 GLU353 GLU419 GLU523
2,4-di-tert-butylphenol (CID-7311)	−7.8	LEU346	MET343, LEU345, LEU346, LEU349, ALA350, MET388, LEU387, LEU384, TRP383, LEU391, VAL392, LEU402, PHE404, VAL418, GLY420, MET421, VAL422, ILE424, PHE425, LEU428, MET517, GLY521, MET522, LEU525, MET528	ASN348 THR347 SER518 HIS524	ARG399 LYS520	GLU353 ASP351 GLU419
2,3-oxidosqualene (CID-5366020)	−8.6		MET342, MET343, GLY344, LEU345, LEU346, LEU349, ALA350, LEU354, TRP383, LEU384, LEU387, MET388, ILE389, LEU391, VAL392, LEU402, PHE404, VAL418, GLY420, MET421, ILE424, PHE425, LEU428, MET517, GLY521, MET522, LEU525, TYR526, MET528, CYS530, VAL533, LEU536	THR347 ASN348 SER518 HIS524	ARG394 LYS520 LYS529 LYS531	ASP351 GLU353 GLU419 GLU523
5,8,11-eicosatriynoic acid, Trimethylsilyl Ester (CID-91696396)	−8.2	Cys530	MET343, LEU346, LEU349, ALA350, LEU354, TRP383, LEU384, ILE386, LEU387, MET388, ILE389, LEU391, VAL392, VAL418, GLY420, MET421, ILE424, PHE425, LEU428, MET517, GLY521, MET522, LEU525, TYR526, MET528, CYS530, VAL533, VAL534, PRO535, LEU536, TYR537, LEU539	THR347 ASN348 SER518 HIS524	ARG394 LYS520 LYS529 LYS531	ASP351 GLU353 GLU380 GLU419
1-monolinolein (CID-250006068)	−8.2		MET343, LEU345, LEU346, LEU349, ALA350, LEU354, CYS381, TRP383, LEU384, LEU387, MET388, ILE389, LEU391, VAL392, VAL418, GLY420, MET421, ILE424, PHE425, LEU428, MET517, GLY521, MET522, LEU525, TYR526, MET528, CYS530, VAL533, VAL534, PRO535, LEU536, TYR537, LEU539	THR347 ASN348 HIS524	ARG394 LYS520 LYS529 LYS531	ASP351 GLU353 GLU380 GLU419 GLU523

3.6. Protein–Ligands Interactions Analysis

For in silico study, the post-docking protein–ligand interaction analysis has made use of the BIOVIA Discovery Studio and Maestro post-docking visualization tool, together with the virtual screening approach, to identify the most notable and tested drug–ligand interactions. With the lowest docking value (−7.8 kcal/mol), CID-7311 collaborated with amino acid sites and formed only one hydrogen bond with Leu346, among other interactions, such as hydrophobic interactions with different amino acids. In terms of the six potential medications, the ligand CID-5366020 had the highest binding energy (−8.6 kcal/mol), forming fourteen hydrophobic connections with the remaining protein residues, identified as MET342, MET343, GLY344, LEU345, LEU346, LEU349, ALA350, LEU354, TRP383, LEU384, LEU387, MET388, ILE389, LEU391, VAL392, LEU402, PHE404, VAL418, GLY420, MET421,

ILE424, PHE425, LEU428, MET517, GLY521, MET522, LEU525, TYR526, MET528, CYS530, VAL533, and LEU536 residues.

Although CID-91696396 possesses a lower binding energy compared to CID-5366020, proficiency includes hydrogen bonds via the 3ERT recipient, specifically two hydrogen bonds using the residue Cys530. This makes CID-91696396 interacting via the 3ERT receptor more powerful and much more effective than CID-5366020. Non-bonded interactions are a fundamental part of drug design techniques, in addition to the fact that non-bonded connections, such as hydrophobic and hydrogen bonds, enhance the durability of both the ligand and the drug and that their number correlates via the interaction of the drug–ligand complex. Additionally, CID-250006068, as well as CID-23725625 (control drug), had an attractive affinity for binding to protein 3ERT receptors (−8.2 kcal/mol and −7.9 kcal/mol, respectively) whilst engaging no hydrogen bond interactions involving the amino acid sites CID-23725625 (control drug), whereas CID-250006068 also has several hydrophobic connections but no hydrogen bonds. All the interacting bonds that were identified among the selected ligands bioactive compounds and targeted proteins complex estrogen receptors alpha (ERα) (PDB ID: 3ERT) are tabulated in Table 4 and Figure 1.

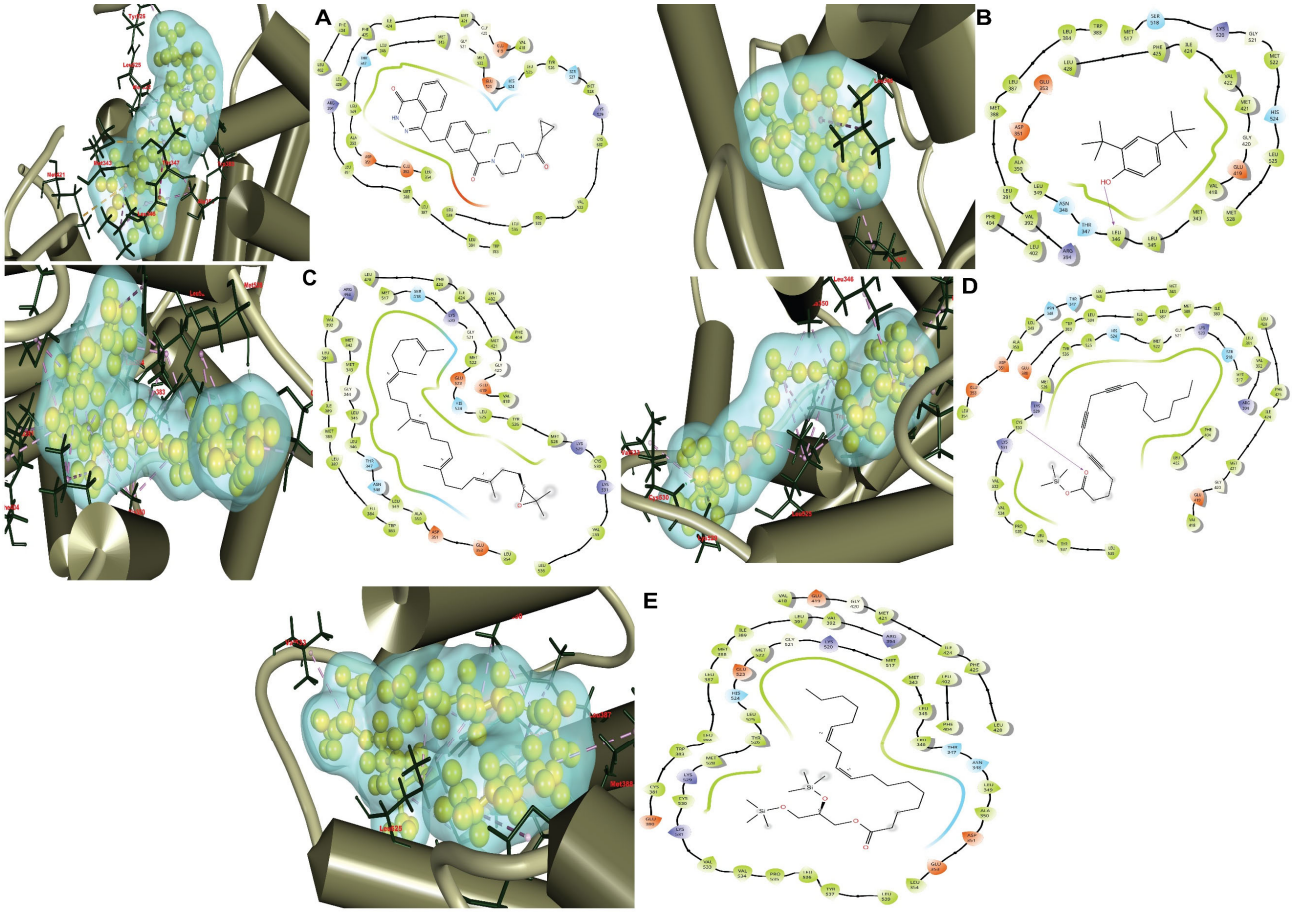


Figure 1. All the evaluated ligand molecules interacted with the estrogen receptor alpha (ERα) protein. The left-hand pictures show the three-dimensional structure of the protein–ligand complex, while the right-hand images show the two-dimensional structure. Here, (**A**) shows the 3D and 2D interactions between the ER protein and the control drug olaparib (CID-23725625), whereas comparative interactions with the ERα protein complex are demonstrated by (**B**) compound 2,4-di-tert-butylphenol (CID-7311); (**C**) compound 2,3-oxidosqualene (CID-5366020); (**D**) compound 5,8,11-eicosatriynoic acid, trimethylsilyl ester (CID-91696396); and (**E**) compound 1-monolinolein (CID-250006068).

3.7. Analysis of MDS Trajectories

To comprehend structural stabilization and intramolecular interactions within protein–ligand complexes in real time, molecular dynamics (MD) modeling is employed in computer-assisted drug development. This method can also determine the conformational shifts of a complex system when subjected to a synthetic environment. This study utilized a 100 ns MD simulation of these proteins in relation to the specific ligand to understand the architectural changes occurring during development. By analyzing the terminal images corresponding to the 100 ns MD simulation trajectories, intermolecular communication connectivity was initially assessed.

3.7.1. RMSD Analysis

The root mean square deviation (RMSD) measurement is a technique used to calculate its median variation in the atom's displacement throughout a specific period in comparison to a benchmark's instant. Within an assortment of 1–3 Å, every protein–ligand interaction's average variation in RMSD is completely reasonable. A major flexible shift in the amino acid structures has taken place whenever the RMSD number is more than 1–3 Å.

As a result, 100 ns MD simulations were performed to evaluate the helical modification for the target polypeptide in its interaction containing the five different ligand molecules represented by CID-250006068, CID-5366020, CID-91696396, CID-7311, and CID-23725625 (control). The normalized RMSD associated with the ligand molecule CID-250006068 ranged from 1.2 to 3.0. The typical RMSD of the ligand substance CID-5366020 ranged from 2.0 to 3.0. The normalized RMSD for the ligand molecule CID-91696396, which had fewer variations, was around 1.2 and 2.8. The normative RMSD for the ligand molecule CID-7311 ranged from 1.2 to 3.2. The average RMSD for the ligand complex CID-23725625 (control) ranged from 1.2 to 3.1. The previous protein–ligand complex arrangement demonstrated translational integrity, as the material's identity fluctuated somewhat as well as being below the permitted threshold (Figure 2).

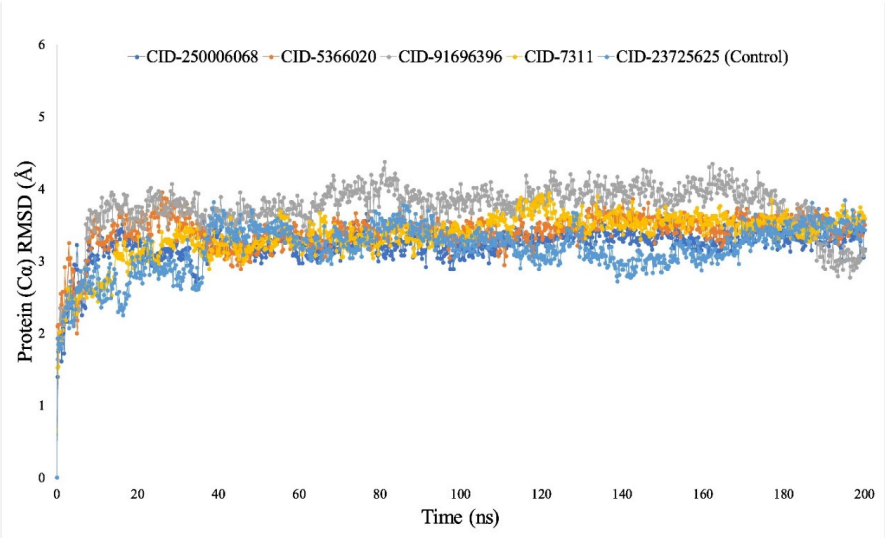


Figure 2. The complicated system's complexity method's recoverable RMSD readings corresponding to the 3ERT proteins modeling incorporating the five ligands' combinations Cα atoms. The selected compounds CID-250006068, CID-5366020, CID-91696396, CID-7311, and CID-23725625 (control) in complex with the protein are represented by blue, orange, gray, yellow, and sky-blue, respectively.

3.7.2. RMSF Analysis

Root mean square fluctuation (RMSF) is a quantitative method for characterizing and identifying local modifications that occur across polypeptide chains when chemicals interact with specific locations in proteins. Whenever ligand chemicals bind to remains, the modifications that take place throughout the chain of amino acids can be determined and

characterized using RMSF. Figure 3 illustrates the determination of the RMSF principles for the substances CID-250006068, CID-5366020, CID-91696396, CID-7311, and CID-23725625 (control) along with intended amino acids simulation to examine how specific substances attach to certain parts of a protein and affect its flexibility. Particularly inflexible intermediate structural components, which include alpha helices together with beta sections, were found with a minimum observation rate ranging from 6 to 230 amino acid repetitions. The greatest amount of variation is seen at the protein's N- and C-termini because of the presence of these domains. Consequently, one may infer that in the simulated environment, the motion of a single atom for each of the five ligand compounds under investigation has a low fluctuation frequency.

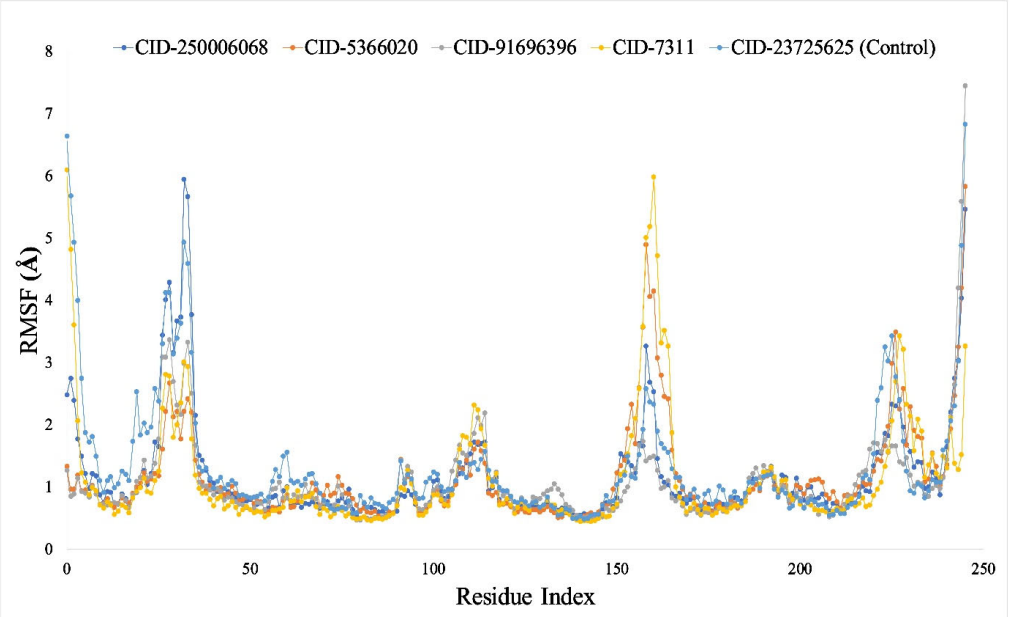


Figure 3. The RMSF readings corresponding to the 3ERT polypeptide modeling corresponding to the five ligand molecules identified in the C atoms of the complex structure. The chosen components CID-250006068, CID-5366020, CID-91696396, and CID-7311, followed by CID-23725625 (control), appear as blue, orange, gray, yellow, and sky-blue in combination with the corresponding protein, sequentially.

3.7.3. Rg Analysis

Every protein–ligand combination platform's atomic distribution across its shaft might be thought of as the radius of gyration (Rg). The calculation of Rg is among the most crucial indicators that predict actual structuring activities of something like a macromolecule and show the variations in overall complex compaction. The configuration of a chemical method's molecules throughout its axis might be used to define the Rg of a protein–ligand relationship. The computation about Rg serves as one of the most important indications to be on the lookout for when forecasting the molecular functioning of a macro molecule since it shows variations in complicated compaction as time goes by. Figure 4 shows the results of this investigation into the durability of CID-250006068, CID-5366020, CID-91696396, CID-7311, and CID-23725625 (control) in connection to the targeted proteins concerning Rg throughout a 100 ns simulation interval. On average, the Rg measurements for the substances CID-250006068, CID-5366020, CID-91696396, CID-7311, and CID-23725625 (control) were discovered to be 5.5, 6.2, 4.1, 3.0, and 5.0, correspondingly, demonstrating the fact that protein's significantly binding pocket is not experiencing substantial alterations in structure over connecting the chosen ligand substances.

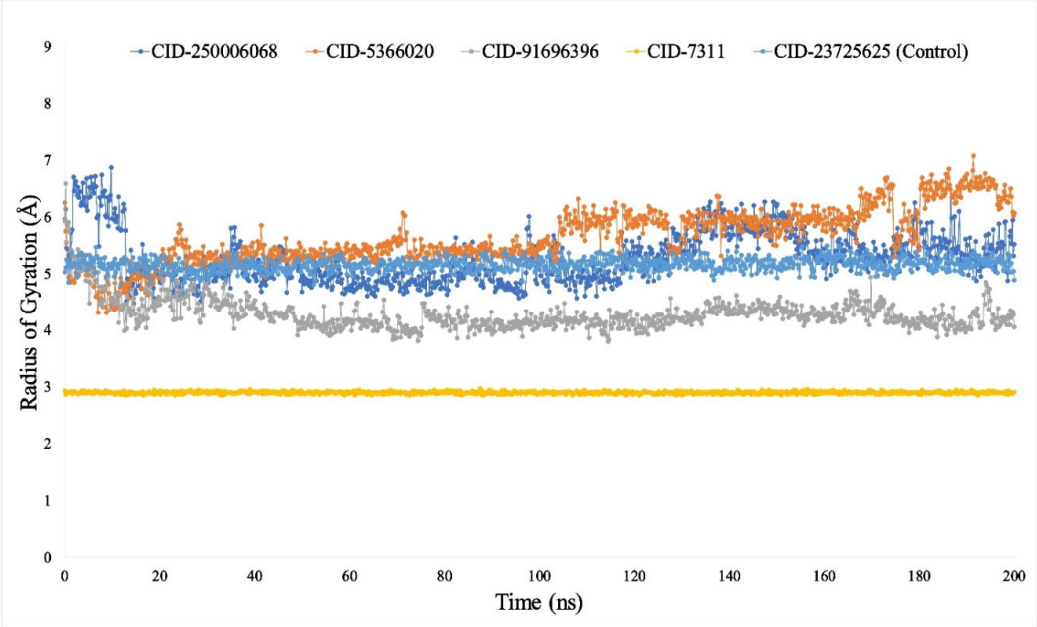


Figure 4. A simulation with a duration of 100 ns to calculate the radius of gyration (Rg). Blue, orange, gray, yellow, and sky-blue represent the selected compounds CID-250006068, CID-5366020, CID-91696396, CID-7311, and CID-23725625 (control) in association with the proteins, respectively.

3.7.4. Analysis of SASA, MolSA and PSA

Solvent surface area affects their formation as well as the functionality underpinning biological macromolecules (SASA). Individual amino acid sequences on a protein's surface normally function as activity domains in the context of protein–ligand complex structures, and they may or may not combine with other molecules, such as receptors. This aids in comprehending the solvent-like properties (hydrophilic or hydrophobic) of a molecule.

The concentration of SASA controls the structure confirmations together with the functioning of physiological biomolecules. The solvent-like qualities of a molecule are better understood when amino acid sequences on its surface operate as active sites and form bonds with other molecules and ligands. The SASA measurement for the peptide complexes, including the five ligands' substances, was consequently calculated and presented in Figure 5. The median SASA readings for the compounds CID-250006068, CID-5366020, CID-91696396, CID-7311, and CID-23725625 (control), ranged from 2 to 2202, suggesting a significant degree of engagement with the amino acid sequence to their chosen chemical in the resulting complex mechanisms.

When using a 1.4 probe diameter, the MolSA is comparable with a van der Waals interface region. The conventional van der Waals region was present during our in silico investigation for CID-250006068, CID-5366020, CID-91696396, CID-7311, and CID-23725625 (control) (Figure 6). Furthermore, solely oxygen, as well as nitrogen atoms, give PSA to molecules. In this instance, a significant PSA result was seen correlated with the targeting proteins in CID-250006068, CID-5366020, CID-91696396, CID-7311, and CID-23725625 (control) (Figure 7).

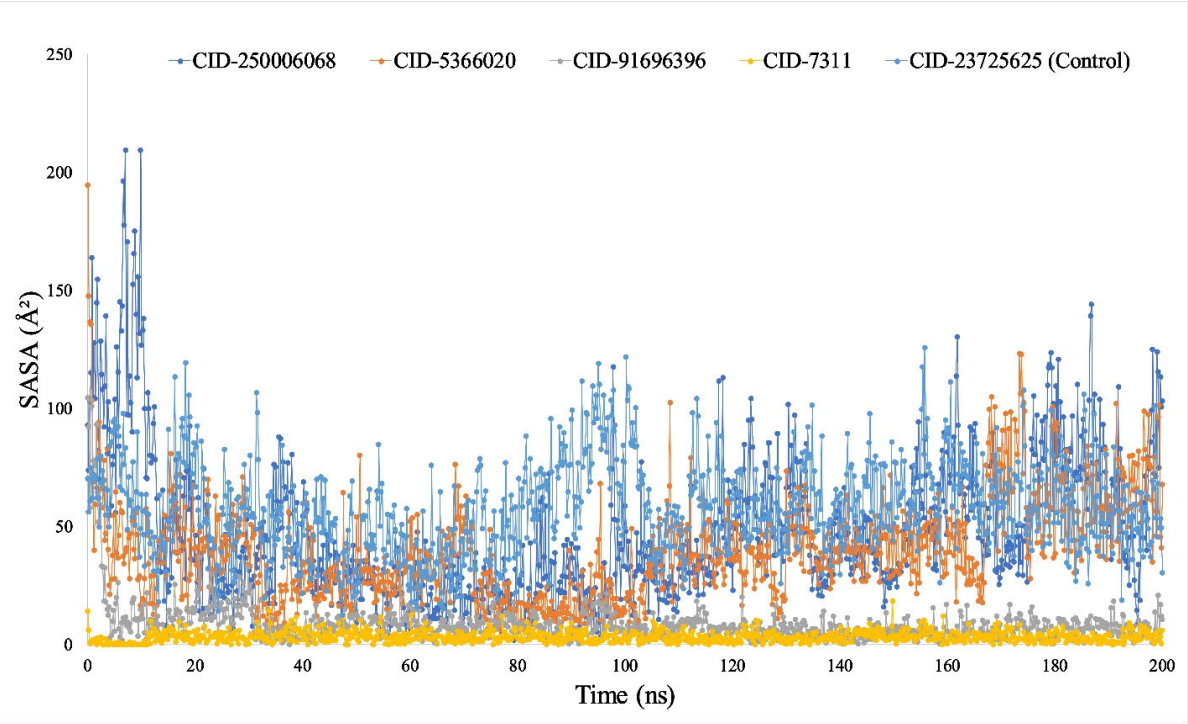


Figure 5. The 100 ns simulated interacting diagram applied to determine the solvent-accessible surface area (SASA) underlying the protein–ligand interacting complexes. The chosen substances CID-250006068, CID-5366020, CID-91696396, and CID-7311, together with CID-23725625 (control), appear as blue, orange, gray, yellow, and sky-blue in combination with the corresponding protein in them, correspondingly.

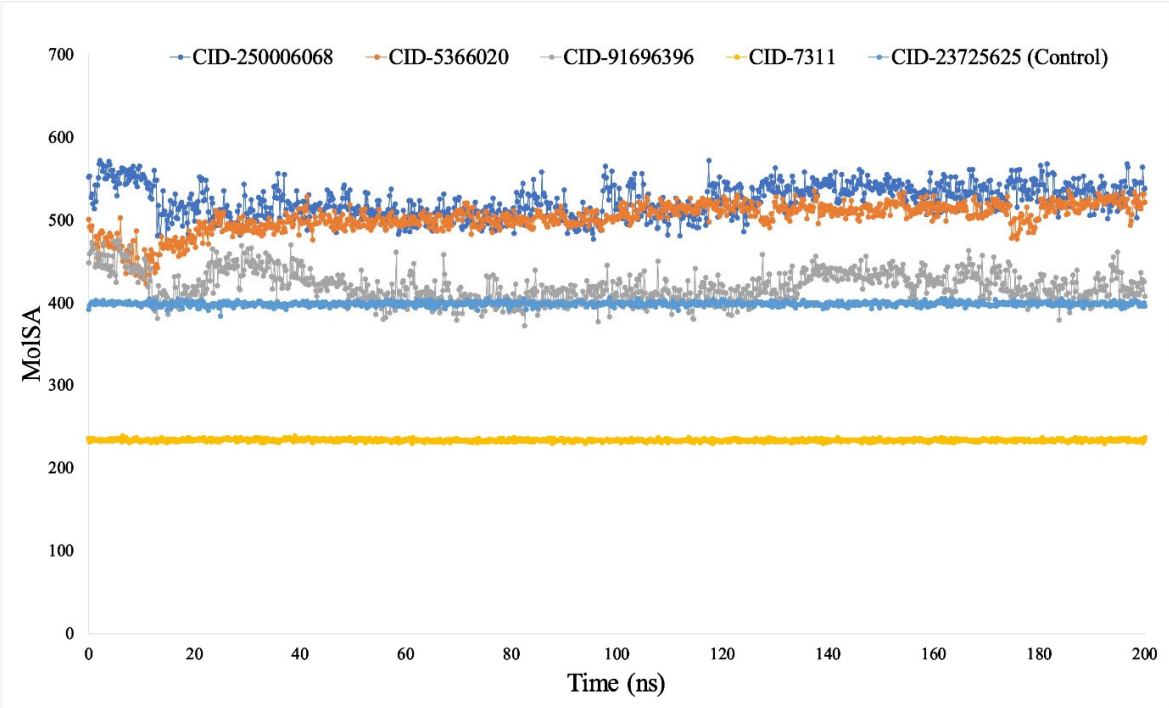


Figure 6. The molecule surface area (MolSA) of the protein–ligand interacting complexes calculated using the 100 ns simulated interaction schematic. The chosen combinations CID-250006068, CID-5366020, CID-91696396, and CID-7311, followed by CID-23725625 (control), are shown as blue, orange, gray, yellow, and sky-blue in combination with the protein content, correspondingly.

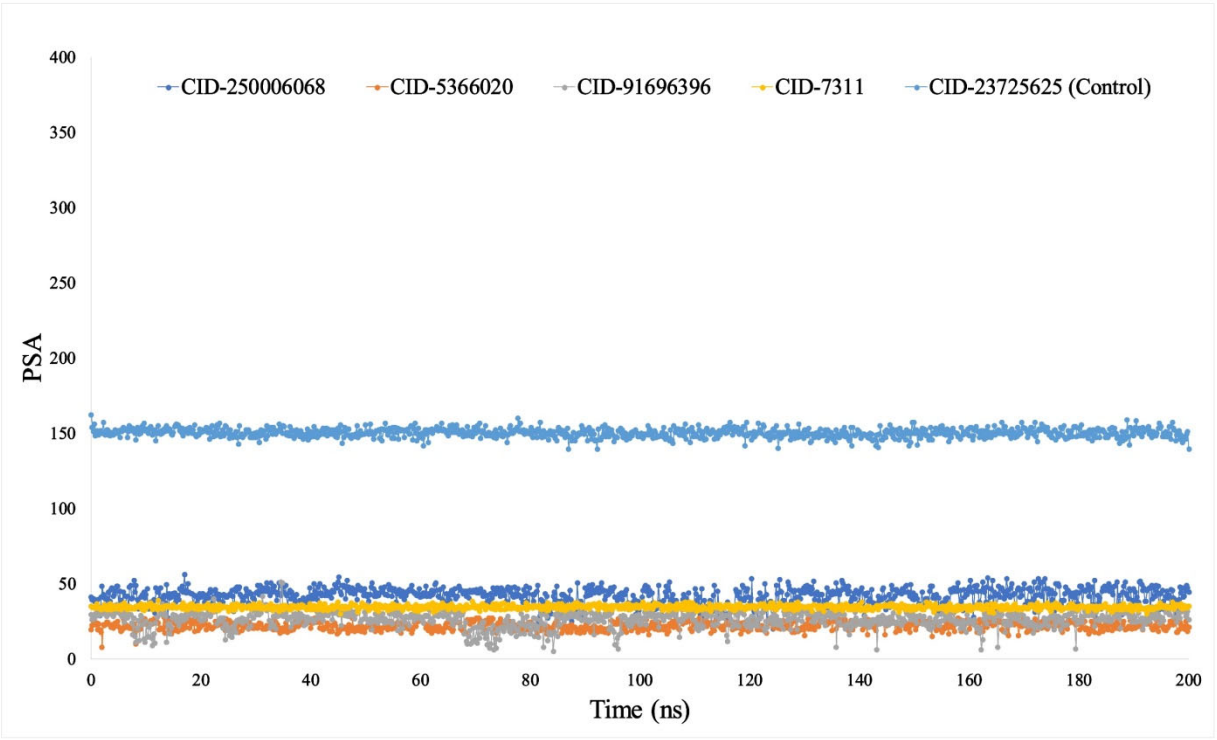


Figure 7. The polar surface area (PSA) of the simulated protein–ligand interactions molecules calculated using 100 ns simulated interaction graphs. The chosen chemicals CID-250006068, CID-5366020, CID-91696396, and CID-7311, together with CID-23725625 (control), are displayed as blue, orange, gray, yellow, and sky-blue in combination with the target protein, respectively.

3.7.5. Analysis of Intramolecular Bonds

To elucidate the discrepancies between molecular docking data and the examination of intramolecular bonds during the 100-nanosecond molecular dynamics (MD) simulation, it is essential to acknowledge the fundamental contrasts between these two approaches. Molecular docking offers a static, short-term forecast of ligand–receptor interactions derived from a singular conformational snapshot of the ligand at the receptor's binding site. It emphasizes evaluating the most probable conformation and interactions, including hydrogen bonds, hydrophobic interactions, and ionic connections, at a specific moment. Nonetheless, these predictions are constrained by the inflexible or semi-inflexible characteristics of most docking algorithms, which fail to consider receptor flexibility or the temporal dynamics of solvent effects.

Conversely, the intramolecular bond analysis derived from molecular dynamics simulation illustrates a dynamic system wherein the flexibility of the ligand, receptor, and solvent molecules is comprehensively accounted for. This offers a more accurate representation of the evolution of interactions throughout time. Hydrogen bonds can be ephemeral, forming and dissociating as the system investigates various conformations. Consequently, a hydrogen bond not detected during docking (for instance, between 1-Monolinolein (CID-250006068) and the receptor) may manifest in the molecular dynamic's simulation owing to the conformational flexibility of the binding site or ligand and vice versa. A hydrogen bond observed in molecular docking (e.g., CID-5366020 with Met528) may not endure throughout the simulation due to structural rearrangements or competing interactions within the dynamic environment (Figure 8).

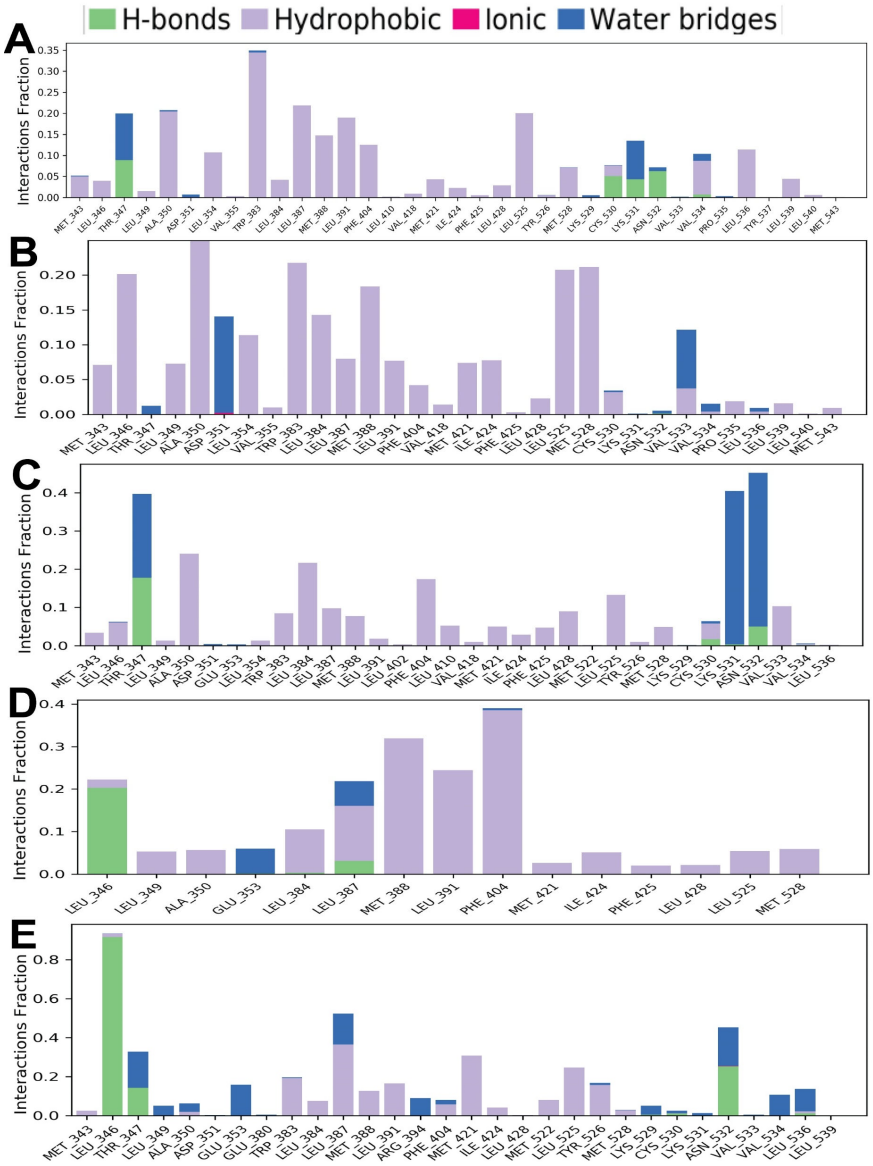


Figure 8. The relationships amongst ligands and protein molecules that were found throughout the 100 ns simulations depicted in layered bar diagrams. This section provides examples of the interactions between the chosen ligand molecules. Wherein CID-250006068, CID-5366020, CID-91696396, and CID-7311, CID-23725625 (control) are the five antagonists that were chosen and are associated with the corresponding protein. In this instance, CID-250006068, CID-5366020, CID-91696396, and CID-7311, CID-23725625 (control) are designated as (**A**–**E**), respectively.

The presence of hydrogen bonds in the MD analysis but their absence in docking for CID-23725625 can be attributed to the time-dependent characteristics of bond formation during simulations. The MD simulation may uncover novel hydrogen bonds when the ligand adjusts to the receptor milieu and refines its interactions in a manner that docking alone cannot anticipate. Moreover, water-bridged hydrogen bonds and other solvent-mediated interactions, typically lacking in docking, are elucidated by molecular dynamics and can substantially enhance overall binding stability.

The disparities between molecular docking and MD simulation illustrate the limitations of static docking models in contrast to the more comprehensive and dynamic representation offered by MD. The distinctions must be examined as a crucial component of comprehending ligand–receptor interactions, as molecular dynamics simulation provides a more comprehensive and precise representation of these complexes within a biological

framework. The distinctions between docking and MD bond analysis highlight the necessity of employing both methodologies in a complementary manner. Molecular docking offers preliminary insights into possible binding modes, but MD modeling enhances these predictions by incorporating system flexibility and solvent dynamics, uncovering transient interactions and a more comprehensive interaction profile over time.

4. Discussion

Since ancient times, people have traditionally sought out plants as a valuable source of diverse bioactive compounds, which hold the potential for treating a wide range of diseases. Phytotherapy, which is based on scientific evidence, is now offering a potent alternative route to the perception of credible natural phytochemicals with no antagonistic effects. The *Croton bonplandianum* extract demonstrates significant levels of phenolic and flavonoid components, along with secondary metabolites such as polyphenols, glycosides, and alkaloids, underscoring its potential as a candidate for anticancer therapeutics. The computer-aided drug design approach has gained significant prominence in recent years due to the way it has demonstrated that it has the potential to speed up the discovery of new pharmaceuticals that are effective and safe [51–53]. This investigation made use of a total of 83 phytocompounds, 4 of which were selected specifically for their potential to act as lead compounds, and the fifth was a substance that was a control drug. The pharmacokinetic properties of these four phytochemicals were computed utilizing web-based servers that the Swiss ADME and pkCSM pharmacokinetics efforts offered, as detailed in Table 1. Drug safety and effectiveness are largely determined by pharmacokinetic characteristics, such as absorption, distribution, metabolism, and excretion (ADME). They eventually impact treatment results by influencing the drug's bioavailability, dosage schedule, and possible adverse effects. It may be possible to create safer and more effective pharmaceuticals by comprehending and improving these qualities [54,55].

In the process of developing new drugs nowadays, scientists heavily rely on in silico drug design approaches. Examining several approaches lowers the expense of finding possible medication candidates by using fewer animal models in pharmaceutical studies. These methods include molecular docking, visualization, homology modeling, and molecular dynamics research [56,57]. Analyzing data acquired from several methodologies employed in the in silico pharmaceutical development process can yield high-quality therapeutic candidates. However, the present pharmaceutical development process requires significant expenses and often encounters numerous undesirable failures at different stages. The primary cause of failure is typically attributed to the limited availability of safety and efficacy, which is commonly related to the properties of absorption, distribution, metabolism, excretion, and toxicity. Additionally, the top five ligands' physiochemical features were analyzed using the Swiss ADME online server. None of the compounds violated the Lipinski rules of five (L5), and they exhibited other favorable properties indicative of a drug-like nature (Table 1). These small molecules demonstrated physiochemical activity, highlighting their potential to interact with the receptor [58]. Alternatively, the analysis of PK (Pharmacokinetics) activity was operated through the web server "pKCSM" [59]; it highlights the compound's absorption, distribution, excretion, and toxicological parameters. Remarkably, the five leads have the highest absorption in the human body.

Computationally, DFT-based QM simulations were carried out to further evaluate and improve the components' geometries. To assess individual substances' molecular aggressiveness, the HOMO-LUMO potential differential based on FMO calculations was also computed. All the substances had significant HOMO-LUMO gaps with energies greater than 0.20 eV, confirming their poor responsiveness in relation to their bioactive components. By employing site-specific super molecular docking to generate a probable binding score, the Maestro application (Schrödinger Release 2021-2: Maestro, Schrödinger, NY, USA, 2020-3) aided in the identification of bioactive phytocompounds exhibiting the most significant and potent binding scores. An experiment into molecular coupling with the targeted protein ERα (PDB ID: 3ERT) included the selection of 83 naturally occurring

bioactive chemicals from *Croton bonplandianum* together with a control drug. Olaparib (CID-23725625), as a control drug, developed a binding affinity of −7.9 kcal/mol. Table 4 shows the binding affinity values of 2,3-oxidosqualene (CID-5366020), 5,8,11-eicosatriynoic acid, trimethylsilyl ester (CID-91696396), 1-Monolinolein (CID-250006068), and 2, 4-Di-tert-butylphenol (CID-7311) among the natural bioactive compounds selected from *Croton bonplandianum*. These values are −8.6 kcal/mol, −8.2 kcal/mol, −8.2 kcal/mol, and −7.8 kcal/mol, respectively. In the subsequent step, Maestro post-docking visualization tool was utilized to analyze the 2D protein–ligand interaction visualization. The state-of-the-art visualizer program BIOVIA Discovery Studio (v19.1.0.18287) also assisted in creating images of the docked receptor–ligand interactions (Figure 1).

Furthermore, dynamic trajectory analysis performance data, also known as molecular dynamic simulation (MDS), can aid in facilitating the development of novel therapeutics [60–62]. In this experiment, we performed 100 ns MDS using the given physiological and physicochemical parameters by utilizing the Desmond Application, a Schrödinger package program. This simulation trajectory was also utilized to analyze the RMSD, RMSF, Rg, hydrogen bond number, and SASA perfectly [63]. The reliability of the protein structure was evaluated, and conformational variations were identified using the alpha carbon and backbone of the selected 3ERT model protein; the lower value denotes the more stable molecule. The significant structural stability of the protein–ligands combined structures is frequently indicated by RMSD values less than 3.5. Our study's findings demonstrated that the RMSD values of the protein–ligand interactions fell within an appropriate range, specifically the average mean value of 3.5, suggesting a more effective docking position and proving that the protein–ligand structure did not exhibit severe fluctuations during the 100 ns molecular dynamics simulation study (Figure 2). RMSF is essential for monitoring local protein modifications since it computes the mean change seen among the atoms and assesses the displacement of an individual atom with respect to the reference structure. To assess the impact of attaching specific ligand molecules to residue positions, we need to measure the alteration in the flexibility of the protein structure. An RMSF graph shows how typical protein fluctuations are a sign of changes at the residue level. The RMSF allows one to calculate typical protein fluctuations from a constant reference point. Figure 3 shows the RMSF for the protein's C-alpha atoms.

The structural stability was evaluated by determining the total number of intermolecular bonds formed between the macromolecule and its ligand compounds. All the selected ligand compounds have a greater number of intramolecular bonds and a more stable conformation than the control drug olaparib (CID-23725625). Along with measuring the size shifts of the drug-like compounds, the solvent-accessible surface area (SASA) of the protein ligands was calculated [64]. Structural instability is a result of hydrophobic amino acid residues being close to the water molecule, which raises the SASA value [65]. The presence of hydrophobic amino acid residues near water molecules induces structural instability, leading to an increase in the SASA value (Figure 5). Validation data for MolSA and PSA demonstrated that each ligand molecule exhibits greater significance compared to the control drug (Figures 6 and 7). Moreover, Rg measurement provides additional insights into the folding properties of the protein and can evaluate the compactness of the protein molecule [66]. Furthermore, a high Rg value indicates slackpacking, while a low Rg value indicates tight packing [67]. A review of the Rg values is shown in Figure 4, which shows that every compound containing the protein showed standard compactness. The findings of molecular dynamics simulation analysis exhibited that the ligand compounds 2,3-oxidosqualene (CID-5366020) and 5,8,11-eicosatriynoic acid, trimethylsilyl ester (CID-91696396) possessed significant stability in every parameter like RMSD, RMSF, Rg, etc. However, the other two selected ligand compounds were omitted from the potent drug candidate list because of reporting unexpected values in different MDS parameters.

5. Conclusions

According to the findings of this computational analysis, the binding affinities of 2,3-oxidosqualene (CID-5366020) and 5,8,11-eicosatriynoic acid, trimethylsilyl ester (CID-91696396) derived from *Croton bonplandianum* were −8.6 kcal/mol and −8.2 kcal/mol, respectively. These values were higher than the binding affinity of the control drug olaparib (CID-23725625), which was −7.9 kcal/mol. Regarding the pharmacokinetic features, it was discovered that both 2,3-oxidosqualene and 5,8,11-eicosatriynoic acid, trimethylsilyl ester had positive ADME profiles, with logP values of 8.55 and 6.40, respectively, and that they were not hazardous. Furthermore, it is worth noting that these compounds exhibited a remarkable level of stability when subjected to molecular dynamics simulations (MDS) with the protein ERα (PDB ID: 3ERT) in comparison to the control drug. Based on the findings of this research, it appears that *Croton bonplandianum* has the potential to serve as a source of therapeutic drugs for the treatment of breast cancer that is ERα-mediated. Additional research should be conducted with the objective of isolating and characterizing the bioactive compounds derived from *Croton bonplandianum*, as well as elucidating the molecular mechanisms of action at play in animal models to validate the therapeutic efficacy of these compounds.

Supplementary Materials: The following supporting information can be downloaded at: https://www.mdpi.com/article/10.3390/app14219878/s1, Table S1: Molecular docking scores and other ADMET properties of all the ligands compounds.

Author Contributions: Conceptualization, M.A.R. and M.N.H.; Data curation, S.S., P.B., M.R.S., S.A.R., M.N.H.Z. and M.N.H.; Formal analysis, S.S., P.B., M.I.T., M.R.S., S.A.R. and M.N.H.Z.; Funding acquisition, M.A.R.; Investigation, M.A.R. and M.N.H.; Project administration, M.N.H.; Resources, P.B.; Software, M.N.H.; Supervision, M.A.R.; Validation, M.N.H.; Visualization, S.S., P.B., M.I.T., M.R.S., M.N.H.Z. and A.H.H.; Writing—original draft, S.S. and P.B.; Writing—review and editing, M.I.T., M.R.S., S.A.R., M.N.H.Z., A.H.H., M.A.R. and M.N.H. All authors have read and agreed to the published version of the manuscript.

Funding: This study did not receive any research grants from public, commercial, or nonprofit funding agencies.

Institutional Review Board Statement: Not applicable.

Informed Consent Statement: Not applicable.

Data Availability Statement: All necessary data generated or analyzed during this study are presented in this article and additional data could be available from the corresponding author upon request.

Acknowledgments: We appreciate the contribution of SeqBee Bioscience, Bangladesh, to providing the analytical tools for our research work. The authors extend their appreciation to Researchers Supporting Project number RSP2024R17, King Saud University, Riyadh, Saudi Arabia.

Conflicts of Interest: The authors declare no conflicts of interest.

References

1. Sharma, R. Breast cancer incidence, mortality and mortality-to-incidence ratio (MIR) are associated with human development, 1990–2016: Evidence from Global Burden of Disease Study 2016. *Breast Cancer* **2019**, *26*, 428–445. [CrossRef] [PubMed]
2. Sohel, M.; Biswas, P.; Al Amin, M.; Hossain, M.A.; Sultana, H.; Dey, D.; Aktar, S.; Setu, A.; Khan, M.S.; Paul, P.; et al. Genistein, a Potential Phytochemical Against Breast Cancer Treatment-Insight into the Molecular Mechanisms. *Processes* **2022**, *10*, 415. [CrossRef]
3. Abd El-Rehim, D.M.; Pinder, S.E.; Paish, C.E.; Bell, J.; Blamey, R.W.; Robertson, J.F.; Nicholson, R.I.; Ellis, I.O. Expression of luminal and basal cytokeratins in human breast carcinoma. *J. Pathol.* **2004**, *203*, 661–671. [CrossRef] [PubMed]
4. Youlden, D.R.; Cramb, S.M.; Dunn, N.A.; Muller, J.M.; Pyke, C.M.; Baade, P.D. The descriptive epidemiology of female breast cancer: An international comparison of screening, incidence, survival and mortality. *Cancer Epidemiol.* **2012**, *36*, 237–248. [CrossRef] [PubMed]

5. Al Saber, M.; Biswas, P.; Dey, D.; Kaium, M.A.; Islam, M.A.; Tripty, M.I.A.; Rahman, M.H.; Rahaman, T.I.; Biswas, M.Y.; Paul, P.; et al. A Comprehensive Review of Recent Advancements in Cancer Immunotherapy and Generation of CAR T Cell by CRISPR-Cas9. *Processes* **2022**, *10*, 16. [CrossRef]
6. Baral, S.K.; Biswas, P.; Kaium, M.A.; Islam, M.A.; Dey, D.; Saber, M.A.; Rahaman, T.I.; Emran, T.B.; Hasan, M.N.; Jeong, M.K.; et al. A Comprehensive Discussion in Vaginal Cancer Based on Mechanisms, Treatments, Risk Factors and Prevention. *Front. Oncol.* **2022**, *12*, 883805. [CrossRef]
7. World Health Organization (WHO). Breast Cancer. Available online: https://www.who.int/news-room/fact-sheets/detail/breast-cancer#:~:text=In%202020,%20there%20were%202.3,the%20world%E2%80%99s%20most%20prevalent%20cancer (accessed on 12 July 2023).
8. Shah, A.N.; Gradishar, W.J. Adjuvant Anthracyclines in Breast Cancer: What Is Their Role? *Oncologist* **2018**, *23*, 1153–1161. [CrossRef]
9. Rivera, E.; Gomez, H. Chemotherapy resistance in metastatic breast cancer: The evolving role of ixabepilone. *Breast Cancer Res. BCR* **2010**, *12* (Suppl. 2), S2. [CrossRef]
10. Wan, X.; Hou, J.; Liu, S.; Zhang, Y.; Li, W.; Zhang, Y.; Ding, Y. Estrogen Receptor α Mediates Doxorubicin Sensitivity in Breast Cancer Cells by Regulating E-Cadherin. *Front. Cell Dev. Biol.* **2021**, *9*, 583572. [CrossRef]
11. Payne, S.J.; Bowen, R.L.; Jones, J.L.; Wells, C.A. Predictive markers in breast cancer—The present. *Histopathology* **2008**, *52*, 82–90. [CrossRef]
12. Fox, E.M.; Davis, R.J.; Shupnik, M.A. ERbeta in breast cancer—Onlooker, passive player, or active protector? *Steroids* **2008**, *73*, 1039–1051. [CrossRef] [PubMed]
13. Levin, E.R. Integration of the extranuclear and nuclear actions of estrogen. *Mol. Endocrinol.* **2005**, *19*, 1951–1959. [CrossRef] [PubMed]
14. Narod, S.A. Hormone replacement therapy and the risk of breast cancer. *Nat. Rev. Clin. Oncol.* **2011**, *8*, 669–676. [CrossRef] [PubMed]
15. Al Azad, S.; Ahmed, S.; Biswas, P.; Mia, M.A.R.; Farjana, M.; Arshe, F.A.; Mily, S.J.; Ankhi, A.B.; Shaikat, M.M.; Sultana, S.; et al. Quantitative analysis of the factors influencing IDA and TSH downregulation in correlation to the fluctuation of activated vitamin D3 in women. *JABET* **2022**, *5*, 320–333. [CrossRef]
16. Khan, A.M.; Sharif, M.A.; Salekeen, R.; Rahman, M.H.; Mahmud, S.; Biswas, P.; Hasan, M.N.; Islam, K.M.D.; Billah, M.M.; Islam, M.E. In vitro and in silico investigation of garlic's (*Allium sativum*) bioactivity against 15-lipoxygenase mediated inflammopathies. *J. Herbmed Pharmacol.* **2023**, *12*, 283–298. [CrossRef]
17. Sanyakamdhorn, S.; Agudelo, D.; Bekale, L.; Tajmir-Riahi, H.A. Targeted conjugation of breast anticancer drug tamoxifen and its metabolites with synthetic polymers. *Colloids Surf. B Biointerfaces* **2016**, *145*, 55–63. [CrossRef]
18. Chang, M. Tamoxifen resistance in breast cancer. *Biomol. Ther.* **2012**, *20*, 256–267. [CrossRef]
19. Subarnas, A.; Diantini, A.; Abdulah, R.; Zuhrotun, A.; Hadisaputri, Y.E.; Puspitasari, I.M.; Yamazaki, C.; Kuwano, H.; Koyama, H. Apoptosis induced in MCF-7 human breast cancer cells by 2′,4′-dihydroxy-6-methoxy-3,5-dimethylchalcone isolated from Eugenia aquea Burm f. leaves. *Oncol. Lett.* **2015**, *9*, 2303–2306. [CrossRef]
20. Cohen, L.H.; Remley, M.J.; Raunig, D.; Vaz, A.D. In vitro drug interactions of cytochrome p450: An evaluation of fluorogenic to conventional substrates. *Drug Metab. Dispos.* **2003**, *31*, 1005–1015. [CrossRef]
21. Society, A.C. *Cancer Facts & Figures*; American Cancer Society: Atlanta, GA, USA, 2016.
22. Elkum, N.; Dermime, S.; Ajarim, D.; Al-Zahrani, A.; Alsayed, A.; Tulbah, A.; Al Malik, O.; Alshabanah, M.; Ezzat, A.; Al-Tweigeri, T. Being 40 or younger is an independent risk factor for relapse in operable breast cancer patients: The Saudi Arabia experience. *BMC Cancer* **2007**, *7*, 222. [CrossRef]
23. Younas, M.; Hano, C.; Giglioli-Guivarc'h, N.; Abbasi, B.H. Mechanistic evaluation of phytochemicals in breast cancer remedy: Current understanding and future perspectives. *RSC Adv.* **2018**, *8*, 29714–29744. [CrossRef] [PubMed]
24. Liu, J.; Schmitz, J.C.; Lin, X.; Tai, N.; Yan, W.; Farrell, M.; Bailly, M.; Chen, T.; Chu, E. Thymidylate synthase as a translational regulator of cellular gene expression. *Biochim. Biophys. Acta* **2002**, *1587*, 174–182. [CrossRef] [PubMed]
25. Dutta, S.; Chaudhuri, T.K. Pharmacological aspect of *Croton bonplandianus* Baill: A comprehensive review. *J. Pharmacogn. Phytochem.* **2018**, *7*, 811–813.
26. Vijayamuthuramalingam, U.D.K.; Rajaram, R.; Kuppusamy, K.M.; Jonnalagadda, B.; Arokiasamy, S. Anti-hyperglycemic and antioxidant potential of *Croton bonplandianus* Bail fractions in correlation with polyphenol content. *Iran. J. Basic Med. Sci.* **2017**, *20*, 1390–1397. [CrossRef]
27. Jeeshna, M.; Paulsamy, S.; Mallikadevi, T.J. Phytochemical constituents and antimicrobial studies of the exotic plant species, *Croton bonplandianum* Baill. *J. Life Sci.* **2011**, *3*, 23–27. [CrossRef]
28. Bhavana, J.; Kalaivani, M.K.; Sumathy, A. Cytotoxic and pro-apoptotic activities of leaf extract of *Croton bonplandianus* Baill. against lung cancer cell line A549. *Indian J. Exp. Biol.* **2016**, *54*, 379–385.
29. Lanchhana, D.S.; Ranjit, M.; Kumar, M.S. Anticancer Activity Study of Some Selected Indian Medicinal Plants Used Traditionally. *J. Pharm. Negat. Results* **2023**, *14*, 1123–1132. [CrossRef]
30. Islam, M.; Rahman, M.; Rahman, M.; Qayum, M.; Alam, M. In vitro evaluation of *Croton bonplandianum* Baill. as potential antitumor properties using Agrobacterium tumefaciens. *J. Agric. Technol.* **2010**, *6*, 79–86.

31. Mahmud, S.; Uddin, M.A.R.; Paul, G.K.; Shimu, M.S.S.; Islam, S.; Rahman, E.; Islam, A.; Islam, M.S.; Promi, M.M.; Emran, T.B.; et al. Virtual screening and molecular dynamics simulation study of plant-derived compounds to identify potential inhibitors of main protease from SARS-CoV-2. *Brief. Bioinform.* **2021**, *22*, 1402–1414. [CrossRef]
32. Biswas, P.; Dey, D.; Rahman, A.; Islam, M.A.; Susmi, T.F.; Kaium, M.A.; Hasan, M.N.; Rahman, M.D.H.; Mahmud, S.; Saleh, M.A.; et al. Analysis of SYK Gene as a Prognostic Biomarker and Suggested Potential Bioactive Phytochemicals as an Alternative Therapeutic Option for Colorectal Cancer: An In-Silico Pharmaco-Informatics Investigation. *J. Pers. Med.* **2021**, *11*, 888. [CrossRef]
33. Biswas, P.; Hasan, M.M.; Dey, D.; Dos Santos Costa, A.C.; Polash, S.A.; Bibi, S.; Ferdous, N.; Kaium, M.A.; Rahman, M.D.H.; Jeet, F.K.; et al. Candidate antiviral drugs for COVID-19 and their environmental implications: A comprehensive analysis. *Environ. Sci. Pollut. Res. Int.* **2021**, *28*, 59570–59593. [CrossRef] [PubMed]
34. Andalib, K.M.S.; Biswas, P.; Sakib, M.R.; Hasan, M.N.; Rahman, M.H.; Habib, A. Identification of novel MCM2 inhibitors from Catharanthus roseus by pharmacoinformatics, molecular docking and molecular dynamics simulation-based evaluation. *Inform. Med. Unlocked* **2023**, *39*, 101251. [CrossRef]
35. Ahmed, S.S.; Rahman, M.O.; Alqahtani, A.S.; Sultana, N.; Almarfadi, O.M.; Ali, M.A.; Lee, J. Anticancer potential of phytochemicals from Oroxylum indicum targeting Lactate Dehydrogenase A through bioinformatic approach. *Toxicol. Rep.* **2023**, *10*, 56–75. [CrossRef] [PubMed]
36. Fang, J.; Liu, C.; Wang, Q.; Lin, P.; Cheng, F. In silico polypharmacology of natural products. *Brief. Bioinform.* **2017**, *19*, 1153–1171. [CrossRef]
37. Ahammad, F.; Tengku Abd Rashid, T.R.; Mohamed, M.; Tanbin, S.; Ahmad Fuad, F.A. Contemporary Strategies and Current Trends in Designing Antiviral Drugs Against Dengue Fever via Targeting Host-Based Approaches. *Microorganisms* **2019**, *7*, 296. [CrossRef]
38. Lu, S.; Ji, M.; Ni, D.; Zhang, J. Discovery of hidden allosteric sites as novel targets for allosteric drug design. *Drug Discov. Today* **2018**, *23*, 359–365. [CrossRef]
39. Kitchen, D.B.; Decornez, H.; Furr, J.R.; Bajorath, J. Docking and scoring in virtual screening for drug discovery: Methods and applications. *Nat. Rev. Drug Discov.* **2004**, *3*, 935–949. [CrossRef]
40. Singh, H.; Bharadvaja, N. Treasuring the computational approach in medicinal plant research. *Prog. Biophys. Mol. Biol.* **2021**, *164*, 19–32. [CrossRef]
41. Mohanraj, K.; Karthikeyan, B.S.; Vivek-Ananth, R.P.; Chand, R.P.B.; Aparna, S.R.; Mangalapandi, P.; Samal, A. IMPPAT: A curated database of Indian Medicinal Plants, Phytochemistry And Therapeutics. *Sci. Rep.* **2018**, *8*, 4329. [CrossRef]
42. Hou, T.; Xu, X. ADME evaluation in drug discovery. 3. Modeling blood-brain barrier partitioning using simple molecular descriptors. *J. Chem. Inf. Comput. Sci.* **2003**, *43*, 2137–2152. [CrossRef]
43. Aribisala, J.O.; S'thebe, N.W.; Sabiu, S. In silico exploration of phenolics as modulators of penicillin binding protein (PBP) 2× of Streptococcus pneumoniae. *Sci. Rep.* **2024**, *14*, 8788. [CrossRef]
44. Bhatia, M.J.C.T. An overview of conceptual-DFT based insights into global chemical reactivity of volatile sulfur compounds (VSCs). *Comput. Toxicol.* **2023**, *29*, 100295. [CrossRef]
45. Klein, J.; Pilmé, J. Exploring the Reactivity of Donor–Acceptor Systems through a Combined Conceptual and Constrained DFT Approach. *J. Chem. Theory Comput.* **2024**, *20*, 2010–2021. [CrossRef]
46. Koltai, P.; Kunde, P. A Koopman–Takens theorem: Linear least squares prediction of nonlinear time series. *Commun. Math. Phys.* **2024**, *405*, 120. [CrossRef]
47. Uzzaman, M.; Hoque, M.J. Physiochemical, molecular docking, and pharmacokinetic studies of Naproxen and its modified derivatives based on DFT. *Int. J. Sci. Res. Manag.* **2018**, *6*, 2018–2025. [CrossRef]
48. Siddiquee, N.H.; Talukder, M.E.K.; Ahmed, E.; Zeba, L.T.; Aivy, F.S.; Rahman, M.H.; Barua, D.; Rumman, R.; Hossain, M.I.; Shimul, M.E.K.; et al. Cheminformatics-based analysis identified (Z)-2-(2,5-dimethoxy benzylidene)-6-(2-(4-methoxyphenyl)-2-oxoethoxy) benzofuran-3(2H)-one as an inhibitor of Marburg replication by interacting with NP. *Microb. Pathog.* **2024**, *195*, 106892. [CrossRef]
49. Yuan, X.-Q.; Yu, X.-H.; Zhu, X.-L.; Wang, X.-C.; Liu, X.-Y.; Cao, J.-W.; Qin, X.-L.; Zhang, P. Comparative Analysis of the Hydrogen Bond Vibrations of Ice XII. *ACS Omega* **2022**, *7*, 2970–2974. [CrossRef]
50. Bowers, K.J.; Chow, E.; Xu, H.; Dror, R.O.; Eastwood, M.P.; Gregersen, B.A.; Klepeis, J.L.; Kolossvary, I.; Moraes, M.A.; Sacerdoti, F.D. Scalable algorithms for molecular dynamics simulations on commodity clusters. In Proceedings of the 2006 ACM/IEEE Conference on Supercomputing, Tampa, FL, USA, 11–17 November 2006; pp. 84–es.
51. Morshed, A.; Al Azad, S.; Mia, M.A.R.; Uddin, M.F.; Ema, T.I.; Yeasin, R.B.; Srishti, S.A.; Sarker, P.; Aurthi, R.Y.; Jamil, F.; et al. Oncoinformatic screening of the gene clusters involved in the HER2-positive breast cancer formation along with the in silico pharmacodynamic profiling of selective long-chain omega-3 fatty acids as the metastatic antagonists. *Mol. Divers.* **2022**, *27*, 2651–2672. [CrossRef]
52. Paul, P.K.; Al Azad, S.; Rahman, M.H.; Farjana, M.; Uddin, M.R.; Dey, D.; Mahmud, S.; Ema, T.I.; Biswas, P.; Anjum, M.; et al. Catabolic profiling of selective enzymes in the saccharification of non-food lignocellulose parts of biomass into functional edible sugars and bioenergy: An in silico bioprospecting. *J. Adv. Vet. Anim. Res.* **2022**, *9*, 19–32. [CrossRef]
53. Rahman, M.D.H.; Biswas, P.; Dey, D.; Hannan, M.A.; Sahabuddin, M.; Araf, Y.; Kwon, Y.; Emran, T.B.; Ali, M.S.; Uddin, M.J. An In-Silico Identification of Potential Flavonoids Against Kidney Fibrosis Targeting TGFβR-1. *Life* **2022**, *12*, 1764. [CrossRef]
54. Jian, J.; He, D.; Gao, S.; Tao, X.; Dong, X. Pharmacokinetics in Pharmacometabolomics: Towards Personalized Medication. *Pharmaceuticals* **2023**, *16*, 1568. [CrossRef] [PubMed]

55. Vora, L.K.; Gholap, A.D.; Jetha, K.; Thakur, R.R.S.; Solanki, H.K.; Chavda, V.P. Artificial Intelligence in Pharmaceutical Technology and Drug Delivery Design. *Pharmaceutics* **2023**, *15*, 1916. [CrossRef] [PubMed]
56. Shaker, B.; Ahmad, S.; Lee, J.; Jung, C.; Na, D. In silico methods and tools for drug discovery. *Comput. Biol. Med.* **2021**, *137*, 104851. [CrossRef] [PubMed]
57. Wadood, A.; Ahmed, N.; Shah, L.; Ahmad, A.; Hassan, H.; Shams, S. In-silico drug design: An approach which revolutionarised the drug discovery process. *OA Drug Des. Deliv.* **2013**, *1*, 3.
58. Gupta, M.; Kant, K.; Sharma, R.; Kumar, A. Evaluation of In Silico Anti-parkinson Potential of β-asarone. *Cent. Nerv. Syst. Agents Med. Chem.* **2018**, *18*, 128–135. [CrossRef]
59. Pasha, M.A.; Mondal, S.; Panigrahi, N.; Shetye, G.; Ma, R.; Franzblau, S.G.; Zheng, Y.T.; Murugesan, S. One-Pot Synthesis of Novel Hydrazono-1,3-Thıazolıdın-4-One Derivatives as Anti-HIV and Anti-Tubercular Agents: Synthesıs, Bıologıcal Evaluatıon, Molecular Modelling and Admet Studıes. *Curr. HIV Res.* **2022**, *20*, 255–271. [CrossRef]
60. Abdullah, A.; Biswas, P.; Sahabuddin, M.; Mubasharah, A.; Khan, D.A.; Hossain, A.; Roy, T.; Rafi, N.M.R.; Dey, D.; Hasan, M. Molecular Dynamics Simulation and Pharmacoinformatic Integrated Analysis of Bioactive Phytochemicals from *Azadirachta indica* (Neem) to Treat Diabetes Mellitus. *J. Chem.* **2023**, *2023*, 4170703. [CrossRef]
61. Aziz, S.; Bibi, S.; Hasan, M.M.; Biswas, P.; Ali, M.I.; Bilal, M.; Chopra, H.; Mukerjee, N.; Maitra, S. A review on influence of biochar amendment on soil processes and environmental remediation. *Biotechnol. Genet. Eng. Rev.* **2023**, *6*, 1–35. [CrossRef]
62. Ferdausi, N.; Islam, S.; Rimti, F.H.; Quayum, S.T.; Arshad, E.M.; Ibnat, A.; Islam, T.; Arefin, A.; Ema, T.I.; Biswas, P.; et al. Point-specific interactions of isovitexin with the neighboring amino acid residues of the hACE2 receptor as a targeted therapeutic agent in suppressing the SARS-CoV-2 influx mechanism. *J. Adv. Vet. Anim. Res.* **2022**, *9*, 230–240. [CrossRef]
63. Krupanidhi, S.; Abraham Peele, K.; Venkateswarulu, T.; Ayyagari, V.S.; Nazneen Bobby, M.; John Babu, D.; Venkata Narayana, A.; Aishwarya, G. Screening of phytochemical compounds of Tinospora cordifolia for their inhibitory activity on SARS-CoV-2: An in silico study. *J. Biomol. Struct. Dyn.* **2021**, *39*, 5799–5803. [CrossRef]
64. Elfiky, A.A.; Elshemey, W.M. Molecular dynamics simulation revealed binding of nucleotide inhibitors to ZIKV polymerase over 444 nanoseconds. *J. Med. Virol.* **2018**, *90*, 13–18. [CrossRef] [PubMed]
65. Mahmud, S.; Rahman, E.; Nain, Z.; Billah, M.; Karmakar, S.; Mohanto, S.C.; Paul, G.K.; Amin, A.; Acharjee, U.K.; Saleh, M.A. Computational discovery of plant-based inhibitors against human carbonic anhydrase IX and molecular dynamics simulation. *J. Biomol. Struct. Dyn.* **2021**, *39*, 2754–2770. [CrossRef] [PubMed]
66. Alamri, M.A.; Altharawi, A.; Alabbas, A.B.; Alossaimi, M.A.; Alqahtani, S.M. Structure-based virtual screening and molecular dynamics of phytochemicals derived from Saudi medicinal plants to identify potential COVID-19 therapeutics. *Arab. J. Chem.* **2020**, *13*, 7224–7234. [CrossRef] [PubMed]
67. Kousar, K.; Majeed, A.; Yasmin, F.; Hussain, W.; Rasool, N. Phytochemicals from selective plants have promising potential against SARS-CoV-2: Investigation and corroboration through molecular docking, MD simulations, and quantum computations. *BioMed Res. Int.* **2020**, *2020*, 6237160. [CrossRef]

Disclaimer/Publisher's Note: The statements, opinions and data contained in all publications are solely those of the individual author(s) and contributor(s) and not of MDPI and/or the editor(s). MDPI and/or the editor(s) disclaim responsibility for any injury to people or property resulting from any ideas, methods, instructions or products referred to in the content.